arXiv:1208.6208v2 [cond-mat.mes-hall] 10 Oct 2012

Giant Spin Hall Effect Induced by Skew Scattering from Bismuth Impurities inside Thin Film CuBi Alloys

Y. Niimi,[1,*] Y. Kawanishi,[1] D. H. Wei,[1] C. Deranlot,[2] H. X. Yang,[3] M. Chshiev,[3] T. Valet,[4] A. Fert,[2] and Y. Otani[1,5]

[1] *Institute for Solid State Physics, University of Tokyo,*
5-1-5 Kashiwa-no-ha, Kashiwa, Chiba 277-8581, Japan
[2] *Unité Mixte de Physique CNRS/Thales, 91767 Palaiseau France associée à l'Université de Paris-Sud, 91405 Orsay, France*
[3] *SPINTEC, UMR CEA/CNRS/UJF-Grenoble 1/G-INP, INAC, 38054 Grenoble, France*
[4] *In Silicio SAS, 730 rue René Descartes, 13857 Aix en Provence Cedex 3, France*
[5] *RIKEN-ASI, 2-1 Hirosawa, Wako, Saitama 351-0198, Japan*

(Dated: October 9, 2012)

We demonstrate that a giant spin Hall effect (SHE) can be induced by introducing a small amount of Bi impurities in Cu. Our analysis based on a new 3-dimensional finite element treatment of spin transport shows that the sign of the SHE induced by the Bi impurities is negative and its spin Hall (SH) angle amounts to −0.24. Such a negative large SH angle in CuBi alloys can be explained by applying the resonant scattering model proposed by Fert and Levy [Phys. Rev. Lett. **106**, 157208 (2011)] to 6*p* impurities.

PACS numbers: 72.25.Ba, 72.25.Mk, 75.70.Cn, 75.75.-c

Spintronic devices manipulating pure spin currents, flows of spin angular momentum without charge current, should play an important role in low energy consumption electronics of next generation. This explains the current interest for the spin Hall effect (SHE) which provides a purely electrical way to create spin currents without ferromagnets and magnetic fields. The SHE, originally predicted by Dyakonov and Perel [1], can be described as an accumulation of spins generated by an electric current on the edges of a nonmagnetic conductor [2]. Its interest in spintronics comes from its application to convert charge into spin currents (or vice-versa). The spin Hall (SH) angle, characteristic of the conversion yield between charge and spin, reaches a few % in heavy metals with strong spin-orbit (SO) interactions such as Pt [3–8].

In addition to the intrinsic SHE of pure metals [8, 9], the skew scattering [10] and the scattering with side-jump [11] on impurities with strong SO interactions can also give rise to the SHE. Such extrinsic mechanisms have already been studied in the SHE induced by nonmagnetic impurities in Cu [12] and in the anomalous Hall effect of ferromagnetic alloys [13]. One of the big advantages for the extrinsic SHE is that it allows controlling the SH angle by changing the combination of host and impurity metals as well as by tuning the impurity concentration. According to recent theoretical predictions [14, 15], some combinations of noble metals and impurities could induce very large SH angles, for example in Cu or Ag doped with Bi. In this work we obtain a large SHE signal in Cu doped with a small amount ($\leq 0.5\%$) of Bi. From our analysis based on a 3-dimensional (3D) finite element treatment of the spin transport equations [16], the SH angle can be estimated to be −0.24 at $T = 10$ K, which is an order of magnitude larger than that in pure metals such as Pt, Pd and almost twice larger than that announced recently for the β phase of Ta [17].

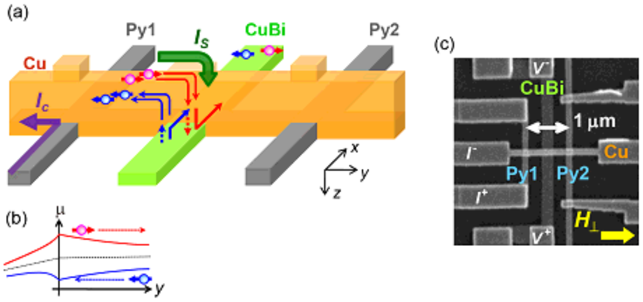

FIG. 1: (Color online) (a) Schematic of the ISHE measurement. The ISHE in CuBi deflects spin-up and down electrons $|e|$ (e is the charge of the electron) denoted by spheres with arrows to the same side. Other arrows indicate the electron motion direction. (b) Electrochemical potential distributions for spin-up and down electrons in Cu. Spin-up and down electrons diffuse in opposite directions, which characterizes a pure spin current (no charge current). (c) Scanning electron microscopy image of our spin Hall device. The yellow arrow in (c) represents the positive direction of the magnetic field in the case of ISHE measurement.

Figure 1(a) shows the principle of the ISHE using the spin absorption method [4, 5, 8, 18, 19]. When the electric current flows from Py1 to the left side of the Cu wire, the resulting spin accumulation induces a pure spin current (no net charge current, i.e. $I_C = 0$ or $I_\uparrow = -I_\downarrow$ for opposite flows of spin-up and down electrons) on the right side of the Cu wire [see Fig. 1(b)]. As discussed later on, most of the pure spin current is absorbed vertically into the middle wire below Cu. The opposite spin-up and down electrons composing the absorbed pure spin current are deflected to the same direction (along the x-axis) by the ISHE in CuBi, and an ISHE voltage V_{ISHE} is generated to prevent the flow of a charge current along

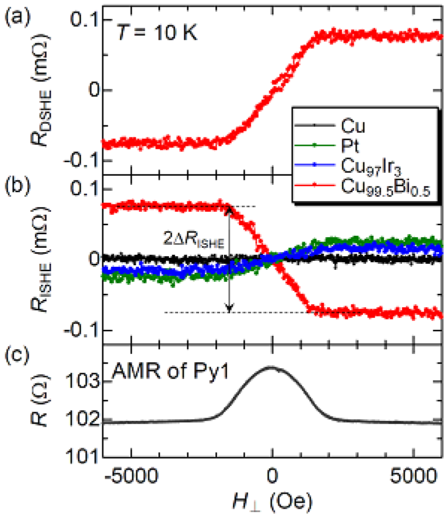

FIG. 2: (Color online) (a) DSHE and (b) ISHE signals of $Cu_{99.5}Bi_{0.5}$ measured at $T = 10$ K. For comparison, the ISHE resistances of a 20 nm thick pure Cu ($\rho = 6.3$ $\mu\Omega$·cm), Pt (10 $\mu\Omega$·cm), and $Cu_{97}Ir_3$ (14 $\mu\Omega$·cm) are also added in (b). (c) A typical AMR signal of Py1 showing the saturation of the magnetization above 2000 Oe for $H_\perp$ along the y direction [see Fig. 1(a)].

the x direction in CuBi. By inverting the probe configuration (i.e. $I^+ \Leftrightarrow V^+$, $I^- \Leftrightarrow V^-$ in Fig. 1(c)), one can also measure the direct SHE (DSHE) [4, 5, 18]; with an electric current in the CuBi wire, the spin accumulation induced at the interface between Cu and CuBi can be detected from the nonlocal voltage between Py1 and Cu.

The ISHE resistance R_{ISHE} ($\equiv V_{\mathrm{ISHE}}/I_{\mathrm{C}}$) as well as the DSHE resistance R_{DSHE} for $Cu_{99.5}Bi_{0.5}$ are plotted in Fig 2, with also reference signals for pure Cu, Pt, and $Cu_{97}Ir_3$. The SHE of Cu is negligibly small but, once only a small amount of Bi is added in Cu, the alloy shows a quite large SHE signal. R_{ISHE} linearly increases with increasing the magnetic field and it is saturated above 2000 Oe which is the saturation field of the magnetization, as can be seen in the anisotropic magnetoresistance (AMR) curve of Fig. 2(c). The amplitude of the SHE resistance is exactly the same for both the DSHE and ISHE, in agreement with the Onsager reciprocal relation [4, 5, 18]. We note the following two points: (I) the sign of R_{ISHE} for CuBi is opposite to that for Pt [4, 5, 8] and $Cu_{97}Ir_3$ [18], and (II) the amplitude (ΔR_{ISHE}) of the ISHE resistance for $Cu_{99.5}Bi_{0.5}$ is several times larger than that of Pt and $Cu_{97}Ir_3$ although their residual resistivities are almost the same ($\rho \sim 10$ $\mu\Omega$·cm), indicating that the SH angle in CuBi is much larger than in Pt and CuIr.

For a quantitative analysis, one has to know how much of the pure spin current I_{S} generated from Py1 is absorbed into the CuBi middle wire. As mentioned above, most of the spin current flowing in Cu is injected into the CuBi wire because of its strong SO interaction, but the rest of the spin current also flows toward the second Py wire (Py2). By measuring nonlocal spin valve (NLSV) signals with and without the middle wire, one can obtain the spin absorption rate into the CuBi wire [5, 8, 18]. Figure 3(a) shows the NLSV signals with and without the $Cu_{99.5}Bi_{0.5}$ wire. With the CuBi wire, the spin accumulation signal $\Delta R_{\mathrm{S}}^{\mathrm{with}}$, defined by the spin accumulation voltage ($\Delta V_{\mathrm{S}}^{\mathrm{with}}$) divided by I_{C}, is reduced to $\sim 50\%$ compared to that without the CuBi wire ($\Delta R_{\mathrm{S}}^{\mathrm{without}}$). The difference between $\Delta R_{\mathrm{S}}^{\mathrm{without}}$ and $\Delta R_{\mathrm{S}}^{\mathrm{with}}$ depends strongly on the spin diffusion length of CuBi, λ_{M}, and can be used to extract λ_{M}, what we have done in two types of model: (A) the standard 1-dimensional (1D) model of diffusive spin transport developed by Takahashi and Maekawa [20] and already used in publications by some of us [8, 18], and (B) a 3D finite element treatment of diffusive spin transport based on an extension of the Valet-Fert formalism to non-collinear spins, SHE and 3D distributions of spin and charge currents (SpinFlow 3D [16]). More details on the two models are presented in supplemental material [19] with a list of the parameters which we use in the 1D and 3D calculations. From the

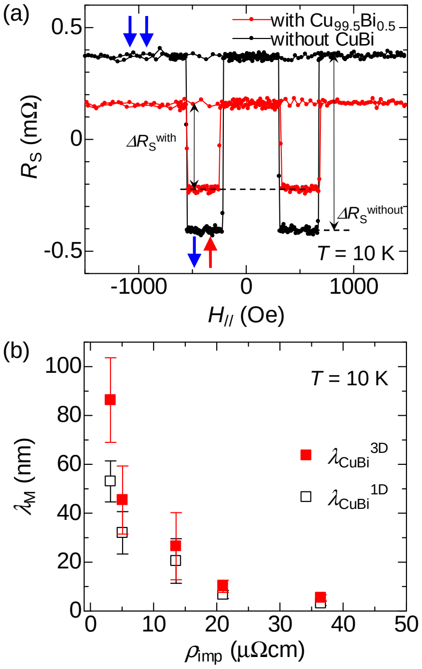

FIG. 3: (Color online) (a) NLSV signals measured at $T = 10$ K with a $Cu_{99.5}Bi_{0.5}$ middle wire (red) and without CuBi wire (black). Arrows represent the magnetization directions of Py1 (left) and Py2 (right). Note that for the NLSV measurement the magnetic field is aligned along the easy axis (x direction) of the Py wires. (b) Spin diffusion length λ_{M} of CuBi alloys at 10 K as a function of ρ_{imp}. Closed and open symbols correspond respectively to the 3D and 1D analyses.

data on $\Delta R_S^{\mathrm{without}}$ and $\Delta R_S^{\mathrm{with}}$ we have derived λ_M in the 1D and 3D models and we present the results in Fig. 3(b). In both models λ_M rapidly decays with increasing the Bi concentration, which expresses the contribution of the Bi impurities to SO-induced spin relaxation. The 3D model gives a longer spin diffusion length for $\lambda_M > t_M$ (thickness of the CuBi wire).

Once λ_M is known, we have used its respective values from the 1D and 3D calculations to derive the SH resistivity ρ_{SHE} in both approaches. In the 1D approach, we used the following standard equation obtained by combining Eqs. (2) and (3) of Ref. [18]:

$$\rho_{\mathrm{SHE}} \simeq \Delta R_{\mathrm{ISHE}} \frac{w_M}{x} \frac{t_M}{\lambda_M} \frac{1-\exp(-2t_M/\lambda_M)}{\{1-\exp(-t_M/\lambda_M)\}^2} \frac{R_N\{\cosh(L/\lambda_N)-1\}+2R_F\{\exp(L/\lambda_N)-1\}+2R_M\sinh(L/\lambda_N)}{2p_F R_F \sinh(L/2\lambda_N)}, \quad (1)$$

where L, w_M, λ_N, and p_F are respectively the distance between Py1 and Py2 (fixed to 1 μm), the width of the CuBi wire, the spin diffusion length of Cu, and the spin polarization of Py, while the spin resistances R_X (X = N, F and M) are defined in Ref. [19]. The determination of the shunting coefficient x has been the object of a recent debate [21] and this is one of the reasons for which we have introduced a 3D modeling to take automatically into account the shunting. As we will see later on, however, the larger deviation of the results of the 1D model from those of the 3D one comes less from the shunting effects than from the spreading of the spin accumulation over the sides of the contacts in the SHE material.

In Fig. 4(a) the SH resistivities of the CuBi alloys derived by our 1D and 3D calculations are plotted as a function of the resistivity induced by the Bi impurities, $\rho_{\mathrm{imp}} \equiv \rho_{\mathrm{CuBi}} - \rho_{\mathrm{Cu}}$. For both calculations the linear variation of the SH resistivity characteristic of skew scattering by dilute impurities is observed only at the lowest concentrations. The large deviation from linearity from $c = 1\%$ and above is consistent with a similar deviation from linearity in the variation of the CuBi resistivity with the Bi concentration [see the inset of Fig. 4(a)] and simply reflects the departure from the dilute impurity regime. We present in Ref. [19] scanning tunneling electron microscopy (STEM) and energy dispersive X-ray (EDX) data showing the inhomogeneous distribution on Bi in the concentrated alloys [22]. Note that the dilute impurity regime is more extended in the CuIr case [18], where both ρ_{SHE} and ρ_{imp} follow linear variations up to Ir concentration 12% [see Fig. 4(b)].

From now we consider only the dilute impurity regime characterized by linear variations of the resistivity and SH resistivity with the concentration. Considering the slope $\rho_{\mathrm{SHE}}/\rho_{\mathrm{imp}}$ in this regime, that is the SH angle α_H characteristic of the skew scattering by Bi impurities [18], we remark that the 3D calculation gives a larger SH angle, $\alpha_H^{3D} = -(0.24 \pm 0.09)$ compared to $\alpha_H^{1D} = -(0.12 \pm 0.04)$. The main reason for this underestimation of the SH angle in the 1D approach is obvious from Fig. 4(c) where one sees the 3D spreading of the spin accumulation on both side edges at the CuBi/Cu junction. This spreading is important when λ_M is longer than t_M. Calculations with the 1D model, in which a pure spin current is injected *only* vertically into the CuBi wire, cannot take into account the spin escape by lateral spreading and thus underestimate the SH angle. The 3D modeling allows to calculate precisely all the contributions coming from local distributions of current and shunting effects around the contacts. The difference between the two models is much smaller for the CuIr alloys where λ_M is in general shorter than t_M and the spin accumulation spreading is less important [see Figs. 4(b) and 4(d)]. The situation is similar for our Pt wire ($\lambda_{\mathrm{Pt}} \sim 10$ nm $< t_{\mathrm{Pt}} = 20$ nm, $\alpha_H^{1D} = 0.021$ and $\alpha_H^{3D} = 0.024$). These results are in contrast to the propositions made by Liu *et al.* [21]; taking into account the 3D effects (shunting, spin accumulation spreading, etc) does not lead to a shorter λ_M. On the contrary λ_M is slightly longer in our 3D treatment, and thus the 1D model underestimates the SH angle (in the present case by a factor of 2), not when λ_M is shorter than t_M but when it is longer. Thus, the important result is the giant SH angle, -0.24, induced by skew scattering on Bi impurities in Cu. This SH angle is the largest value as far as we know, definitely above the range $0.12 - 0.15$ recently found in Au [23] and Ta [17]. Note that $\alpha_H = -0.24$, obtained by dividing ρ_{SHE} by ρ_{imp}, is the characteristic SH angle of the skew scattering on Bi. When ρ_{SHE} is divided by $\rho_{\mathrm{CuBi}} (= \rho_{\mathrm{Cu}} + \rho_{\mathrm{imp}})$, the global SH angle of the alloy becomes -0.11. The value $\alpha_H = -0.24$ would be obtained by using the copper of smaller residual resistivity (less defect and thicker film).

The large SH angle predicted by a recent *ab*-initio calculation for CuBi alloys [14] is consistent with our experiment but the signs are opposite. To clear up the issue, we have tried another theoretical approach adapting the phase shift model worked out by Fert and Levy [15] for 5d impurities to the case of Bi. We start with an *ab*-initio calculation (using Quantum-ESPRESSO [24]) of the numbers of electrons at $j = 1/2$ and $j = 3/2$ p-states in the conduction band on the Bi site (see Ref. [19]

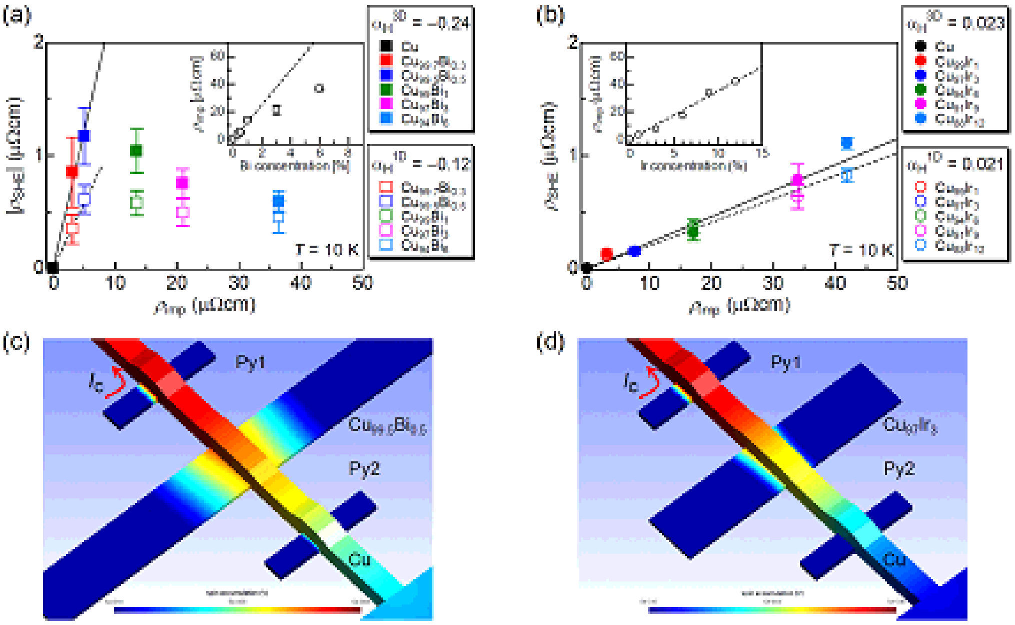

FIG. 4: (Color online) (a) SH resistivity of CuBi alloys as a function of $\rho_{\rm imp}$. Closed and open symbols correspond respectively to the 3D and 1D analyses. The SH angles $\alpha_{\rm H}^{\rm 3D}$ and $\alpha_{\rm H}^{\rm 1D}$ correspond to the slopes of solid and broken lines, respectively. The inset shows the resistivity induced by Bi impurities $\rho_{\rm imp}$ as a function of Bi concentration. (b) For comparison, the SH resistivity of CuIr alloys is plotted as in (a), but the experimental data are derived from Fig. 3 in Ref. [18]. The linear variation of the SH resistivity with $\rho_{\rm imp}$ is not limited by the solubility of Ir up to concentrations as large as 12%. (c), (d) 3D mappings of the spin accumulation voltage for the (c) $\rm Cu_{99.5}Bi_{0.5}$ and (d) $\rm Cu_{97}Ir_3$ SH devices calculated with SpinFlow 3D [16].

for more details). By comparing with the numbers of p-conduction electrons on a Cu site, we find the numbers of electrons attracted on a Bi site and derive the $j = 1/2$ and $j = 3/2$ scattering phase shifts ($\eta_{1/2}$ and $\eta_{3/2}$) from Friedel's sum rule. The difference in these phase shifts comes from the SO interaction and induces the SHE. The phase shift η_0 of the $l = 0$ channel is also found from the *ab*-initio calculations. A straightforward extension of the formalism developed in Ref. [15] for d to p states leads to the following expression of the SH angle:

$$\alpha_{\rm H} = \frac{-2\sin\eta_0\left\{\sin\eta_{1/2}\sin\left(\eta_{1/2}-\eta_0\right)-\sin\eta_{3/2}\sin\left(\eta_{3/2}-\eta_0\right)\right\}}{3\left(\sin^2\eta_0+\sin^2\eta_{1/2}+2\sin^2\eta_{3/2}\right)}. \tag{2}$$

The final result for the SH angle of CuBi alloy is −0.046. The negative sign is in agreement with our experimental results and the SH angle is large but not as large as in the experiments. However, it can be further increased, for example, by taking into account electron correlation effects which may significantly enhance the SO splitting as recently proposed by Gu *et al* [23]. Indeed, we have checked that an increase of the splitting between the $\eta_{1/2}$ and $\eta_{3/2}$ phase shifts by a factor of about 3 keeps the right sign but would bring the SH angle beyond −0.26.

Finally one wonders if interfacial effects could also contribute to our experimental results. The possible competition between the SHE and the interfacial Rashba effects has indeed been debated recently [25, 26] for the interpretation of experiments with 2 ∼ 3 nm thick Pt layers. For our thicker CuBi films (20 nm), the SHE contribution can be expected to be largely predominant. Also some enhancement of the SHE at interfaces [27] can be neglected in a 20 nm thick metallic film in which the interface states cannot exceed a couple of atomic layers.

In conclusion, we find that a small amount of Bi impurities (≤ 0.5%) in Cu induces a large SHE. We have analyzed our data using both the classical 1D model of previous SHE studies and a 3D finite element treatment of spin transport. A large SH angle is derived from both models. It is definitely larger in the 3D model (−0.24).

Such a difference between 1D and 3D models is not surprising since the 3D model can treat more accurately the unavoidable approximations of the 1D model. Harnessing such a giant SHE to produce or detect spin currents will be probably more and more used in novel generations of spintronic devices not necessarily based on magnetic materials.

We acknowledge helpful discussions with I. Mertig, M. Gradhand, S. Maekawa, T. Ziman, B. Gu, and A. Smogunov. We would like to thank Y. Iye and S. Katsumoto for the use of the lithography facilities and also P. M. Levy for the derivation of Eq. (2). This work was supported by KAKENHI, the Agence Nationale de la Recherche, and a Grant-in-Aid for Scientific Research in Priority Area from MEXT.

---

* Electronic address: niimi@issp.u-tokyo.ac.jp

[1] M. I. Dyakonov and V. I. Perel, Phys. Lett. A **35**, 459 (1971).

[2] Y. K. Kato *et al.*, Science **306**, 1910 (2004).

[3] E. Saitoh *et al.*, Appl. Phys. Lett. **88**, 182509 (2006).

[4] T. Kimura *et al.*, Phys. Rev. Lett. **98**, 156601 (2007).

[5] L. Vila *et al.*, Phys. Rev. Lett. **99**, 226604 (2007).

[6] O. Mosendz *et al.*, Phys. Rev. Lett. **104**, 046601 (2010).

[7] L. Liu *et al.*, Phys. Rev. Lett. **106**, 036601 (2011).

[8] M. Morota *et al.*, Phys. Rev. B **83**, 174405 (2011).

[9] T. Tanaka *et al.*, Phys. Rev. B **77**, 165117 (2008).

[10] J. Smit, Physica (Amsterdam) **24**, 39 (1958).

[11] L. Berger, Phys. Rev. B **2**, 4559 (1970).

[12] A. Fert *et al.*, J. Magn. Magn. Mat. **24**, 231 (1981).

[13] A. Fert and O. Jaoul, Phys. Rev. Lett. **28**, 303 (1972).

[14] M. Gradhand *et al.*, Phys. Rev. Lett. **104**, 186403 (2010); Phys. Rev. B **81**, 245109 (2010).

[15] A. Fert and P. M. Levy, Phys. Rev. Lett. **106**, 157208 (2011).

[16] The analysis has been performed using SpinFlow 3D based on the Valet-Fert model; T. Valet and A. Fert, Phys. Rev. B **48**, 7099 (1993).

[17] L. Liu *et al.*, Science **336**, 555 (2012).

[18] Y. Niimi *et al.*, Phys. Rev. Lett. **106**, 126601 (2011).

[19] See supplemental material at ...

[20] S. Takahashi and S. Maekawa, Phys. Rev. B **67**, 052409 (2003); Sci. Technol. Adv. Mater. **9**, 014105 (2008).

[21] L. Liu *et al.*, arXiv:1111.3702.

[22] D. J. Chakrabarti and D. E. Laughlin, Bull. Alloy Phase Diagrams **5**, 148 (1984).

[23] B. Gu *et al.*, Phys. Rev. Lett. **105**, 216401 (2010).

[24] P. Giannozzi *et al.*, J. Phys: Condens. Matter **21**, 395502 (2009); www.quantum-espresso.org

[25] I. M. Miron *et al.*, Nature (London) **476**, 189 (2011).

[26] L. Liu *et al.*, arXiv:1110.6846.

[27] D. Hou *et al.*, Appl. Phys. Lett. **101**, 042403 (2012).